Luminescent Probes

DOI: 10.1002/ange.201302564

Activatable Probes Based on Distance-Dependent Luminescence Associated with Cerenkov Radiation**

*Nalinikanth Kotagiri, Dariusz M. Niedzwiedzki, Kohtaro Ohara, and Samuel Achilefu**

Optical imaging techniques have evolved from basic preclinical applications to an enabling clinical technology platform for the diagnosis and treatment of human diseases. A major bottleneck for the clinical translation of light-based imaging and therapeutic techniques is the limited penetrability of light into deep tissue. This drawback has led to widespread attention and renewed interest in Cerenkov emission, especially in the area of molecular imaging, as a tissue-depth-independent spontaneous light source.[1] Cerenkov radiation (CR) is a photophysical phenomenon in which continuous wave (CW) light in the 250–600 nm range is emitted by charged particles, such as positrons and electrons, traveling faster than light in a dielectric medium with a refractive index of >1.[2] Generally, appreciable CR is produced as a byproduct of the highly energetic radionuclides or external beam radiation used in various clinical interventions. However, owing to significant tissue autofluorescence, the absorption and scattering of UV and visible light, Cerenkov luminescence imaging (CLI) faces steep challenges, such as rapid signal attenuation and low fluence rates. Thus, coupling CR with fluorophores that emit in the optical window at wavelengths in the range of 650–950 nm will minimize tissue autofluorescence and enhance the detection of light from deep tissue.

Recently, positron emission tomography (PET) isotopes such as copper-64 (^{64}Cu), fluorine-18 (^{18}F) and gallium-68 (^{68}Ga), as well as external beam irradiators, such as clinical linear accelerators, have been used to excite fluorophores both in vitro and in vivo.[3] Unfortunately, the CW emission of CR increases the probability of photobleaching organic dyes, which generally have low photostability and narrow absorption spectra for efficient energy transfer from Cerenkov emission. In this regard, quantum dots (QDs) are viable alternatives to organic dyes because of their excellent photostability, high quantum yield, large Stokes shifts, and broad excitation spectra that can capture both the UV and visible light from CR.[4] Recent reports have shown that CR can excite QDs both in vitro and in vivo through Cerenkov radiation energy transfer, where CR serves as the energy donor and the QDs as the energy acceptor.[3b,5] These studies were based on the random interactions between CR and fluorophores.

In this study, we explored the potential application of CLI in the development of activatable probes by programming and controlling the distance between fluorophore and radionuclide. To develop activatable probes and a hybrid "nanoruler" based on Cerenkov-radiation-associated distance-dependent luminescence, we designed new molecular beacons using QDs as CR acceptors, DNA as a spacer, and ^{64}Cu as a source of CR. Both QDs and DNA offer significant advantages to developing molecular rulers.[6] Three prerequisites are essential for the success of this design: 1) specificity, 2) programmability, and 3) rigidity; DNA uniquely possesses these attributes. The programmable nature of DNA self-assembly serves as an excellent platform for developing molecular probes and beacons. Unlike conventional FRET, CR energy transfer can occur over a long range, requiring the consideration of the persistence length of DNA (the length of DNA that behaves as a rigid rod) needed to maintain the validity of the distance-based model. The persistence length is ca. 5 nm for single stranded (ss) DNA and 10 times higher for double stranded (ds) DNA (ca. 50 nm, or 100 base pairs) at a given salt concentration.[7] Therefore, we used DNA hybridization systems that maintained linearity over the model range to minimize coiling or flexibility that resulted in the inaccuracies observed in previous ssDNA models.[8]

The probe design consists of streptavidin-coated QD655 that was conjugated to biotin-modified 99-base-long ssDNA (99 mer). Streptavidin-coated QDs were used primarily to provide rigidity to the design, because other modifications, such as carboxyl and amine functions, are typically conjugated to the QD surface using flexible PEG linkers, thus opening the possibility for misalignment of DNA. Seven 10-base-long ssDNA (10 mer) sequences complementary to the 99 mer were designed to anneal distinctly at bases 1–10, 7–17, 15–25, 30–40, 44–54, 59–69, and 88–98 on the 99 mer, where 1 is closest to the QD. Assuming that the distance between two adjacent base pairs is 0.34 nm, the estimated distance of the respective anneal locations of the 10 mers corresponds to 1.15 nm, 3.65 nm, 6.15 nm, 11.15 nm, 16.15 nm, 21.15 nm, and 31.15 nm. In calculating the metric distances, the length of the

[*] Dr. N. Kotagiri, K. Ohara, Prof. Dr. S. Achilefu
Department of Radiology, Washington University School of Medicine, 4525 Scott Avenue, St. Louis, MO 63110 (USA)
E-mail: achilefus@mir.wustl.edu
Homepage: http://www.orl.wustl.edu
Dr. D. M. Niedzwiedzki
Photosynthetic Antenna Research Center, Washington University in St. Louis, One Brookings Drive, St. Louis, MO 63130 (USA)

[**] This study was supported in part by grants from the US National Institutes of Health (NIBIB R01 EB008111, NCI R01 CA171651 and SIG 1S10RR031625-01) and the National Science Foundation (CCF 0963742). Time-resolved fluorescence and absorption experiments were performed in Ultrafast Laser Facility of the Photosynthetic Antenna Research Center (PARC), an Energy Frontier Research Center funded by the U.S. Department of Energy (DE-SC 0001035). We thank Dr. Mikhail Berezin, Dr. Monica Shokeen, Dr. Yuan-Chuan Tai, and Sergey Komarov for helpful discussions.

Supporting information for this article is available on the WWW under http://dx.doi.org/10.1002/anie.201302564.

linkers used for the bioconjugation was also considered. Non-cross-hybridizing sequences were selected to prevent any errors in the probe assembly process.[9] A chelator with a functional azide group, 1,4,7,10-tetraazacyclododecane-1,4,7,10-tetraacetic acid (DOTA), was attached to the 10 mers that controls the distance of the chelated radionuclide from the QD surface (Figure 1). Owing to its optimal half-life (12.7 h) and significant Cerenkov emission, ^{64}Cu was used to

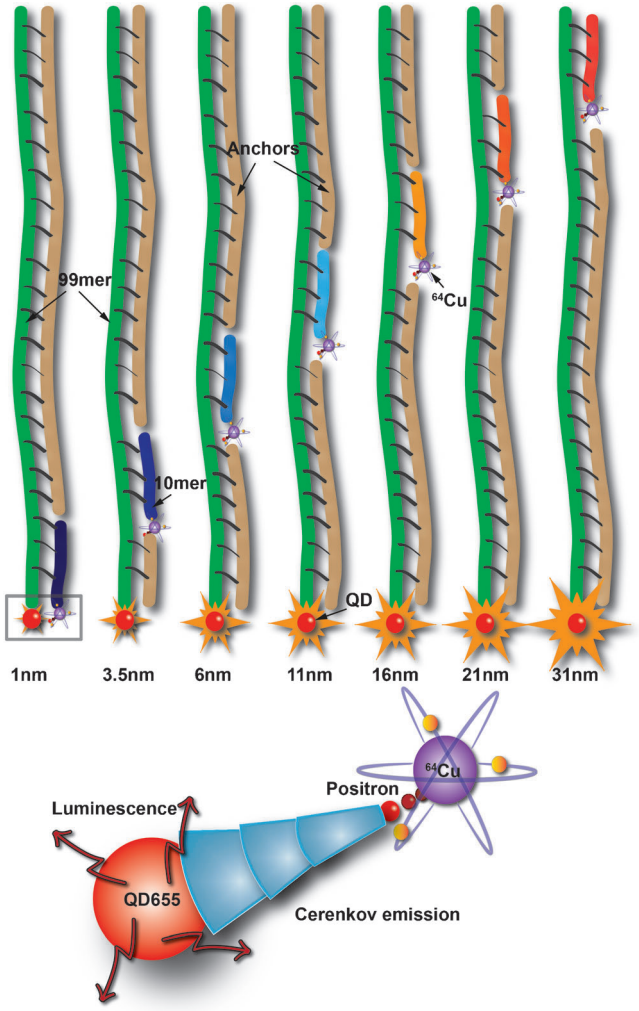

Figure 1. Nanoruler design using QD conjugated to 99 mer ssDNA and seven 10 mer ssDNA sequences with ^{64}Cu, which anneal at distinct distances from the QD surface. Positrons and electrons emit Cerenkov radiation that excites QD655 for luminescence imaging (not drawn to scale).

implement the design. A copper free [2+3] cycloaddition strategy (click chemistry) was used for bioconjugation. This strategy was primarily chosen for its simplicity, high selectivity in aqueous media, prevention of non-specific Cu adducts, modularity, and stability of the reactants and final products.[10] Amino-group-modified 10 mer ssDNA (0.8 μM) was activated with DBCO-PEG$_4$-NHS ester (DBCO = dibenzylcyclooctyne, PEG = poly(ethylene glycol), NHS = *N*-hydroxysuccinimide) and conjugated to azide–DOTA after chelation with ^{64}Cu (ca. 50 μCi, 156.25 nM). The seven unique 10 mer ssDNA sequences were similarly prepared for annealing with the QD–99 mer adducts. Complementary ssDNA "anchors" were designed to hybridize to the 99 mer to ensure maintenance of a persistent dsDNA throughout the entire length of the 99 mer (Figure 1). Moreover, the electrostatic repulsion between the phosphate groups of the multiple ssDNA copies on each QD favors long persistence rigidity.

Distance measurements of ^{64}Cu–DOTA–ssDNA (10 mer) at specified locations on the 99 mer-QD adduct were determined through luminescence using an IVIS Lumina XR multimodal image capturing system (Supporting Information, Figure S3). All experiments were performed in buffered aqueous solutions to maintain the persistence length of DNA. The positive control, which consisted of an admixture of QDs and ^{64}Cu–DOTA without DNA linkers, generated maximum radiance in the Cy5.5 channel (690 nm–770 nm). No significant radiance was observed from the wells containing ^{64}Cu–DOTA alone in this channel. At 1 nm distance, QD emission was 33 ± 5 % of the initial (control) value, which is the lowest radiance value observed in our model. Increasing the distance between the radionuclide and the QD surface from 1 nm to 31 nm resulted in a significant increase in the emission (Figure 2). In comparison to the control, the corresponding values were (41 ± 6) %, (47 ± 3) %, (49 ± 3) %, (52 ± 3) %,

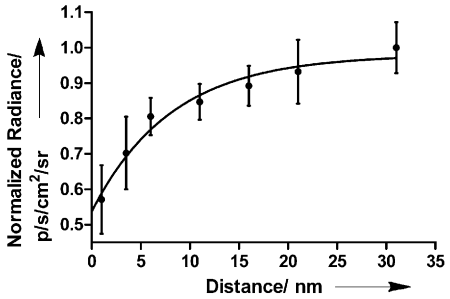

Figure 2. Plot depicting the exponential increase in QD655 radiance as a function of ^{64}Cu distance from the QD surface. Non-linear regression fitting analysis was applied after background correction. Radiance was normalized to the maximum value.

(55 ± 5) %, and (58 ± 4) % for 3.5 nm, 6 nm, 11 nm, 16 nm, 21 nm, and 31 nm, respectively.

The above trend suggests the existence of distance-dependence in CR-induced luminescence, which is attributable to a variety of factors. As Cu^{II} is known to quench the fluorescence of organic dyes, QDs and fluorescent proteins,[11] we investigated the effect of Cu^{II} on the QD signal attenuation. There was no noticeable difference in the QD655 radiance between the DOTA-chelated or unchelated (free) ^{64}Cu (data not shown). However, fluorometric titrations of unchelated "cold" Cu^{II} with QD655 revealed a 25 % reduction in the emission at a molar ratio of 1:1 (Figure S4). In contrast, only a 13 % reduction in luminescence was found for unlinked chelated Cu^{II}. This can be attributed to enhanced contact quenching as a result of random collisions between Cu^{II} ions and the QD surface. However, the probability of contact quenching occurring in the QD–DNA–Cu constructs

is low because of the presence of multiple rigid dsDNAs per particle. This prompted further investigation into the possible distance-dependent quenching effect of ionic copper. Distance studies using DNA-linked "cold" DOTA–Cu^{II} showed the QD emission reduced to $(56\pm5)\%$ of the initial value at 1 nm. The corresponding values were $(64\pm5)\%$, $(75\pm3)\%$, $(77\pm7)\%$, $(79\pm5)\%$, $(84\pm8)\%$, and $(93\pm6)\%$ for 3.5 nm, 6 nm, 11 nm, 16 nm, 21 nm, and 31 nm, respectively (Figure 3a). Based on these findings, the quenching phenomenon is likely due to a photoinduced electron-transfer process, or energy transfer, or a combination of these factors.

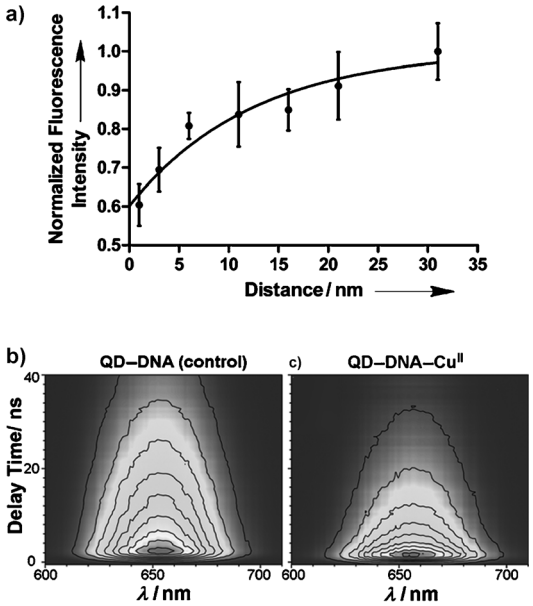

Figure 3. a) Plot depicting the validation of the distance-based model with cold Cu^{II} through steady-state fluorescence-intensity measurements. Non-linear regression fitting analysis was applied. b) TRF of the QD–DNA without Cu^{II}. c) TRF of the QD–DNA attached to Cu^{II} at a distance of 1 nm from QD.

To better understand the underlying phenomenon, picosecond time-resolved fluorescence (TRF) spectroscopy studies were conducted. Figure 3b and c show, respectively, the fluorescence decay contours of QD–DNA (denoted as control) and QD–DNA–Cu^{II} with the Cu cation attached to the DNA strand at a distance of 1 nm from the QD nanoparticle. Both samples were measured under identical conditions, but the difference in fluorescence decay of both samples is evident. Thus, the presence of Cu^{II} in the vicinity of the QD influences the emissive recombination of the photogenerated electron–hole pairs. The results of data fitting shown in Figure S6 demonstrate that density of the electron–hole pairs, which recombine with the emission of photons, is relatively low.

Furthermore, the fluorescence decay has primarily exponential character, with a decay rate constant ($k=2.7\times10^{-2}\,(\mathrm{ns})^{-1}$) corresponding to a fluorescence lifetime (τ) of 38.4 ns (see the Supporting Information for details). In contrast, the proportion of this component was reversed for QD–DNA–Cu^{II}, with the exponentially decaying component (Figure S6) accounting for only 25% of initially emitted (at $t=0$) photons. Domination of the second order decay character in the fluorescence dynamics of QD–DNA–Cu^{II} suggests that the initial concentration of the deeply trapped electrons responsible for the emission of photons during the recombination process is significantly higher than in the QD–DNA control sample. This result is surprising because such an effect can be achieved by increasing excitation intensity. However, the excitation intensity remained exactly the same during all TRF measurements. Alternatively, a similar effect could be expected if the mobility of the photogenerated carriers is increased through the so-called trap-filling effect.[12] Probably, the observed phenomenon can be achieved by introducing an additional non-radiative recombination path for photogenerated electrons that are still in the conduction band, which do not contribute to fluorescence. This should decrease the carrier density and increase the mobility of non-trapped electrons and holes, accelerate the trapping process, and trigger a non-exponential decay of fluorescence. This putative path suggests an ultrafast electron transfer to Cu^{II} from QD through DNA, which facilitates charge separation, and which is followed by rapid non-radiative recombination with a non-trapped hole. This sequence of events leads to charge recombination from the valence band in the QD.

Detailed characteristics of the kinetic components obtained from the fluorescence-decay fitting of the samples with Cu^{II} attached at different distances from the QD are provided in Table S1. No clear relationship between the decay rates and the distance between QD and Cu^{II} was found. However, the decay rate of the exponential component is clearly larger for all Cu^{II}-attached samples compared to the control. The lifetime of the exponentially decaying component of the fluorescence decay shortens from 38.4 ns to an average value of 28.6 ns. It also suggests that some sort of resonant energy transfer between the QD nanoparticle and Cu^{II} occurs and provides an additional non-radiative decay path for excitation and additional fluorescence quenching. A Cu^{II} absorption spectrum taken in buffered solution exhibits a broad featureless band spanning both visible and NIR regions, which substantially overlaps with the QD655 emission spectrum (Figure S5). The overlap provides direction for energy funneling, thus making energy transfer between QD and Cu^{II} energetically feasible. However, due to the low molar extinction coefficient of Cu^{II} ($\varepsilon_{750}=1.20\times10^{4}\,\mathrm{dm^3\,mol^{-1}\,cm^{-1}}$), the contribution of energy transfer towards quenching QD is most likely minimal.

Some of the events in the early delay times after excitation cannot be resolved by TRF measurements. To obtain this additional information, femtosecond time-resolved absorption spectroscopy (TRA) was applied (see the Supporting Information for details). However, no significant differences in the transient absorption spectra and dynamics between the samples was observed (Figure S7). These results are less surprising. The intensity of the amplified laser beam used for TRA is ca. 3000 times higher than that used for TRF measurements. Unfortunately, under such conditions subtle differences in excited state dynamics expected to be observed are masked by the overwhelming trap-filling effect induced by high-intensity excitation.

We therefore suggest that the QD–DNA–^{64}Cu construct undergoes static quenching with electron transfer as the dominant phenomenon. Duplex DNA is known to assist ultrafast short- and long-range electron-transfer processes through its π-framework, which is facilitated by base stacking.[13] However, a DNA strand could also mediate the observed quenching. Distance-dependent quenching has been reported for ethidium/rhodium intercalators as donor/acceptor pair in duplexes DNA and hairpins.[14] To assess the possible contribution of DNA to QD quenching, we directly labeled streptavidin-coated QDs with biotin–DOTA–^{64}Cu, without using DNA assembly. QD–streptavidin admixed with azide–DOTA–^{64}Cu was used as a control. Streptavidin–biotin interfacial platforms have been used as bridges for electron transfer.[15] The observed radiance of the QD–avidin–biotin–DOTA–^{64}Cu complex was ca. 41 % of the control (Figure S8). This quenching efficiency is similar to that observed for DNA assembled at 1 nm from the QD surface, which suggests that the DNA does not contribute significantly to the observed quenching phenomenon. Also, we did not observe any change in radiance when the QD–99 mer construct, without the complementary 10 mer strand, was admixed with azide–DOTA–^{64}Cu. Furthermore, a full-length complementary 99 mer ssDNA with a DBCO internal modification at the 88th base, which corresponds to a distance of 31 nm, was used to correlate the luminescence and fluorescence measurements with the 10 mer and anchor-based design at the same distance. Essentially, no significant difference between the 99 mer- and 10 mer-based designs was observed in both the luminescence (^{64}Cu) and fluorescence (Cu^{II}), measurements (Figure S9). By conforming to the distance-based model, these findings suggest that the quenching efficiency is influenced by the length of the linkers used for connecting the electron donor to the electron acceptor, as long as they maintain the electron transfer process.

Therefore, the distance dependent changes observed in QD luminescence when using ^{64}Cu is primarily driven by the quenching efficiency of Cu^{II} through ultrafast electron transfer. This places ^{64}Cu in a unique position among PET isotopes, because of its potential to serve both as a light source through CR and a broad-range luminescence quencher through energy and photoinduced electron-transfer mechanisms. This dual role could maximize the utility and performance of optical–nuclear-activatable probes powered by CR.

To validate this model, we used both the strand-displacement hybridization and hairpin probe approaches. Strand displacement hybridization, also known as a Yin Yang probe, fundamentally operates in the same way as a hairpin probe, where the fluorophore (QDs) on 3′ end of ssDNA is in close proximity to a quencher on the 5′ end of its complementary sequence.[16] In a hairpin probe, both of these sequences form the stem, and are connected by a looped ssDNA sequence that is usually designed to complement the target ssDNA (Figure 4a). In the strand displacement model, we observed a (45 ± 7.5) % increase in radiance after annealing the target 60 mer to the 99 mer, displacing the 10 mer–DOTA–^{64}Cu complex (Figure 4b).

When an activatable probe is envisaged, obtaining the highest SNR is highly desired. In the case of strand-displacement probes, the design aims to release the isotope completely into the surrounding milieu. This implies that the sphere of influence will play a deterministic role in obtaining a high SNR. The sphere of influence can be loosely defined as the volume of liquid in the immediate vicinity of the isotope in which the photon flux of the CR is optimal for exciting fluorophores. Currently, the sphere of influence for individual PET isotopes is uncertain. Factors such as the diffusion rate, half-life, and the internal dynamics of cellular events could contribute to the redistribution of an isotope and the diffusion of fluorophores away from the sphere of influence. In such cases, real-time tracking of the probe to record the activation event will be required. This can be especially challenging for detection systems in vivo. Using a hairpin probe could obviate this potential problem.

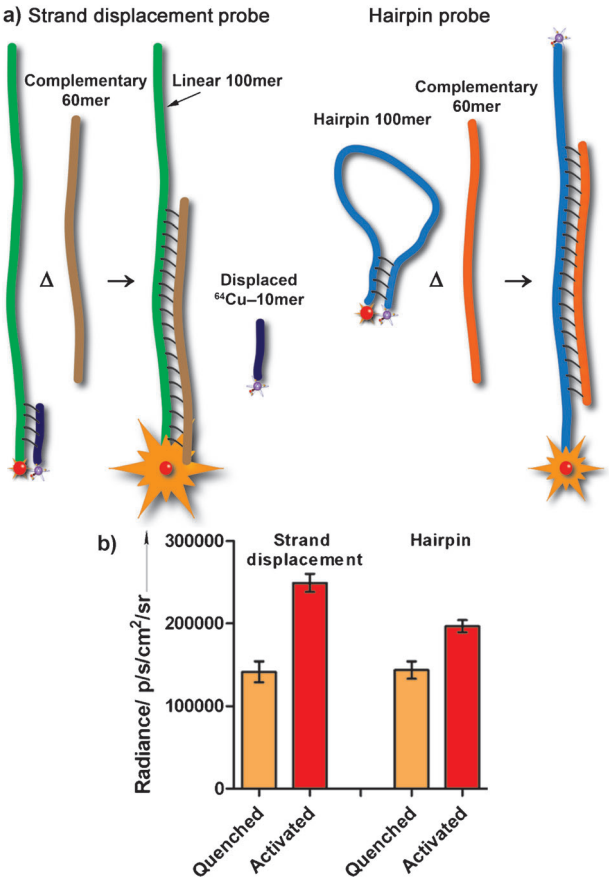

Figure 4. a) Strand-displacement and hairpin probes. b) Comparison of luminescence readings for the strand-displacement probe and the hairpin probe after a target DNA hybridization activation event.

In the hairpin-probe design, a 100 mer was used to simulate the 1.15 nm distance construct in its native state and the 31 nm distance construct after annealing with its target and linearization. The 5′ end was biotinylated for binding with QD-streptavidin and the 3′ end was modified with an amine group to allow for conjugation of a DBCO-based linker for use in a click reaction with azide–DOTA. Upon annealing with its 60 mer complement, a luminescence increase of (22 ± 6.5) % relative to the initial value was observed (Figure 4b). This agrees with the ca. 25 % increase

observed in our model nanoruler, where there was ca. 33% and ca. 58% quenching at 1.15 nm and 31 nm, respectively, relative to the control. Although a complete quenching of luminescence would be desirable prior to probe activation, the background luminescence could facilitate tracking of the probes using in vitro and in vivo systems. However, complete luminescence quenching and higher activation luminescence can be obtained by incorporating a dark quencher labeled with ^{64}Cu, and by using DNA probes exceeding 30 nm, respectively.

In summary, we have demonstrated the feasibility of utilizing ^{64}Cu to design and construct optical nanorulers and activatable probes. The design was based on using DNA as a linker to control the distance of ^{64}Cu from the QD655 surface. Short DNA 10 mers were used for annealing on a 90 mer at seven distinct locations, ranging from 1–31 nm from the QD surface. The increase in radiance at 1 nm and 31 nm was ca. 33% and ca. 58%, respectively, relative to the initial value. The results suggest that luminescence quenching was mediated by ultrafast CR-induced electron transfer from the QD to Cu^{II}. This model was validated by using strand displacement model, where a ca. 45% increase in luminescence upon activation was observed compared to the hairpin model, which had a modest ca. 22% increase relative to the initial value. The ensemble of the results holds promise for the potential use of the distance model to report molecular processes. The usable working life of ^{64}Cu-based probes will be determined by the initial activity achieved after probe assembly and by the sensitivity of the imaging system. The relatively short half-life of ^{64}Cu and the activity (< 150 μCi) used to develop the probes described in this study can be classified as relatively non-hazardous and slightly "radiotoxic". However, safety considerations are required for handling radioisotopes under all circumstances, and all of the experiments with radioactive materials were conducted with the approval of the Washington University Radiation Safety Committee.

Received: March 27, 2013
Published online: June 13, 2013

Keywords: activatable DNA probes · Cerenkov radiation · luminescence · nanorulers · quantum dots

[1] a) R. Robertson, M. S. Germanos, C. Li, G. S. Mitchell, S. R. Cherry, M. D. Silva, *Phys. Med. Biol.* **2009**, *54*, N355–65; b) H. Liu, G. Ren, Z. Miao, X. Zhang, X. Tang, P. Han, S. S. Gambhir, Z. Cheng, *PLoS One* **2010**, *5*, e9470; c) A. E. Spinelli, C. Kuo, B. W. Rice, R. Calandrino, P. Marzola, A. Sbarbati, F. Boschi, *Opt. Express* **2011**, *19*, 12605–18; d) Z. Hu, X. Ma, X. Qu, W. Yang, J. Liang, J. Wang, J. Tian, *PLoS One* **2012**, *7*, e37623.
[2] J. V. Jelley, *Br. J. Appl. Phys.* **1955**, *6*, 227–232.
[3] a) J. Axelsson, S. C. Davis, D. J. Gladstone, B. W. Pogue, *Med. Phys.* **2011**, *38*, 4127–4132; b) R. S. Dothager, R. J. Goiffon, E. Jackson, S. Harpstrite, D. Piwnica-Worms, *PLoS One* **2010**, *5*, e13300.
[4] X. Michalet, F. F. Pinaud, L. A. Bentolila, J. M. Tsay, S. Doose, J. J. Li, G. Sunderesan, A. M. Wu, S. S. Gambhir, S. Weiss, *Science* **2005**, *307*, 538–544.
[5] H. Liu, X. Zhang, B. Xing, P. Han, S. S. Gambhir, Z. Cheng, *Small* **2010**, *6*, 1087–91.
[6] a) F. Morgner, D. Geibler, S. Stufler, N. G. Butlin, H.-G. Lohmannsroben, N. Hilebrandt, *Angew. Chem.* **2010**, *122*, 7732–7736; *Angew. Chem. Int. Ed.* **2010**, *49*, 7570–7574; b) R. Chhabra, J. Sharma, H. Wang, S. Zou, S. Lin, H. Yan, S. Lindsay, Y. Liu, *Nanotechnology* **2009**, *20*, 485201.
[7] J. B. Hays, M. E. Magar, B. H. Zimm, *Biopolymers* **1969**, *8*, 531–536.
[8] W. J. Parak, T. Pellegrino, C. M. Micheel, D. Gerion, S. C. Williams, A. P. Alivisatos, *Nano Lett.* **2003**, *3*, 33–36.
[9] R. Deaton, J.-W. Kim, J. Chen, *Appl. Phys. Lett.* **2003**, *82*, 1305–07.
[10] M. D. Best, *Biochemistry* **2009**, *48*, 6571–84.
[11] a) J. Brunner, R. Kraemer, *J. Am. Chem. Soc.* **2004**, *126*, 13626–7; b) Y. Chen, Z. Rosenzweig, *Anal. Chem.* **2002**, *74*, 5132–8; c) Y. Rahimi, A. Goulding, S. Shrestha, S. Mirpuri, S. K. Deo, *Biochem. Biophys. Res. Commun.* **2008**, *370*, 57–61.
[12] T. Yoshihara, R. Katoh, A. Furube, Y. Tamaki, M. Murai, K. Hara, S. Murata, H. Arakawa, M. Tachiya, *J. Phys. Chem. B* **2004**, *108*, 3817–3823.
[13] a) J. K. Barton, C. V. Kumar, N. J. Turro, *J. Am. Chem. Soc.* **1986**, *108*, 6391–6393; b) C. Wan, T. Fiebig, S. O. Kelley, C. R. Treadway, J. K. Barton, A. H. Zewail, *Proc. Natl. Acad. Sci. USA* **1999**, *96*, 6014–6019.
[14] a) S. O. Kelley, E. Holmlin, E. D. A. Stemp, J. K. Barton, *J. Am. Chem. Soc.* **1997**, *119*, 9861–9870; b) F. D. Lewis, T. Wu, Y. Zhang, R. L. Letsinger, S. R. Greenfield, M. R. Wasielewski, *Science* **1997**, *277*, 673–676.
[15] O. Azzaroni, M. Alvarez, M. Mir, B. Yameen, W. Knoll, *J. Phys. Chem. C* **2008**, *112*, 15850–15859.
[16] Q. Li, G. Luan, Q. Guo, J. Liang, *Nucleic Acids Res.* **2002**, *30*, e5.

